Single-Particle Study of Pt-Modified Au Nanorods for Plasmon-Enhanced Hydrogen Generation in Visible to Near-Infrared Region

Zhaoke Zheng, Takashi Tachikawa,*,[†] and Tetsuro Majima*

The Institute of Scientific and Industrial Research (SANKEN), Osaka University, Mihogaoka 8-1, Ibaraki Osaka 567-0047, Japan

S *Supporting Information*

ABSTRACT: Pt-modified Au nanorods (NRs) synthesized by anisotropic overgrowth were used for producing H_2 under visible and near-infrared light irradiation. The Pt-tipped sample exhibited much higher activity compared with fully covered samples. Using single-particle spectroscopies combined with transmission electron microscopy, we observed obvious quenching phenomena for photoluminescence and light scattering from individual Pt-tipped NRs. The analysis of energy relaxation of plasmon-generated hot electrons indicates the electron transfer from the excited Au to Pt.

Photocatalysis has received significant attention for the direct conversion of solar energy to chemical energy and is being utilized in applications such as environmental cleaning, CO_2 reduction, and hydrogen (H_2) production.[1−3] However, some of the major constraints of this process include low photocatalytic efficiency and limited visible-light photoabsorption. Moreover, stable photocatalysts that produce H_2 under visible light are rare. Therefore, it is important to develop an efficient photocatalyst that harvests a wide range of solar radiation.

Recently, surface plasmon resonance (SPR) of Au nanoparticles (NPs) has been applied to visible-light-responding photocatalysts. SPR can be described as the photoinduced collective oscillation of conduction band electrons. The resonant light wavelength and SPR intensity are dependent on the metal and the size and shape of the metallic nanostructure.[4−7] Among the nanostructures used for photocatalysis, Au nanorods (NRs) with broadly tunable aspect-ratio-dependent longitudinal surface plasmon resonance (LSPR) have been used to improve the absorption because of its wide range of visible-light harvesting.[8,9] Surface plasmons decay either by radiative scattering of resonant photons or by the formation of excited (hot) electrons, which can induce surface photochemical reactions of the adsorbates.[10] The intrinsic ultrafast energy relaxation of hot electrons in the metal can compete with the charge transfer from the metal NPs. To maximize the charge separation of hot electrons in the Au NPs, Au can be coupled with efficient electron acceptors such as TiO_2 and graphene.[9,11] However, the quantum efficiency for H_2 formation over such systems is still relatively low.[12] Compared to monometallic particles, bimetal heterostructures exhibit enhanced catalytic properties and stabilities.[13] Nevertheless, the utilization of bimetal heterostructures in the field of photocatalysis has been rarely reported. Recently, Pd-modified Au

NRs have been reported to exhibit enhanced catalytic activity for chemical reactions upon plasmon excitation.[14] Thus, disparate metals with high work functions can be introduced as efficient electron acceptors for enhancing charge separation. Furthermore, compared to homogeneous core−shell structures, anisotropic overgrowth of metal heterostructures is advantageous for catalytic reactions.[15] Anisotropic metal heterostructures can be obtained by lateral etching of core−shell nanorods or site-selective silica coatings.[15,16] Because of the stronger interaction of surface-capping molecules such as cetyltrimethylammonium bromide (CTAB) with the {110} facets of Au NRs, CTAB bilayers are closely packed at the sides than at the ends.[17] This phenomenon can be utilized for the anisotropic overgrowth of metal heterostructures.

In this study, we developed an efficient route for the anisotropic overgrowth of Pt on Au NRs using a binary surfactant mixture consisting of CTAB and 5-bromosalicylic acid. The Pt-tipped Au NRs and fully covered samples were successfully synthesized by altering the side-coating surfactants. The Pt-modified Au NRs were used for producing H_2 under visible and near-infrared (NIR) light irradiation. The efficiency of hot electron transfer between the Au NRs and the Pt cocatalyst were investigated by single-particle photoluminescence (PL) and dark-field scattering (DFS) spectroscopies combined with transmission electron microscopy (TEM). Because the chemical synthesis of anisotropic metal nanostructures often yields a broad distribution of sizes, shapes, and constituents, single-particle analyses are essential to exclude undesirable effects caused by sample heterogeneity and impurities. To further support our conclusions, we performed computational simulation using the finite difference time domain (FDTD) method.

Figures 1a and S1 show the TEM images of Au NRs synthesized using CTAB and 5-bromosalicylic acid. The NRs obtained were 50 ± 6 nm in length and 13 ± 2 nm in diameter (aspect ratio of 3.8 ± 0.4), and they gave rise to an LSPR peak centered at about 788 nm (Figure 1b). In the FDTD calculation, the cylindrical Au NRs capped with two half spheres at the ends were assumed to have an average value of 50×14 nm. The calculated LSPR peak centered around 774 nm was in good agreement with our experimental data (Figure S2a). Figure 1c shows the TEM images of Pt-covered Au NRs with an initial Pt concentration of 25 mol %. Because the cohesive interaction of Pt atoms is higher than the adhesive interaction between Au and Pt atoms, Pt exhibits the island
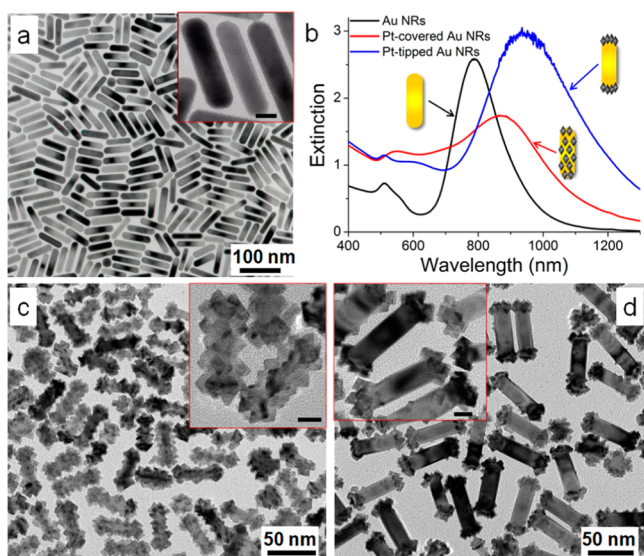
Figure 1. TEM images of (a) Au NRs and (c) Pt-covered and (d) Pt-tipped Au NRs. (b) UV−vis−NIR extinction spectra of the three samples with the same concentration. Scale bars in the insets represent 10 nm.

Figure 2. (a) Time course of H_2 evolution from water−methanol (20 vol %) suspensions of Pt-modified Au nanoparticles (0.188 mg) under visible-light irradiation ($460 < \lambda < 820$ nm). (b−d) Extinction spectra and action spectra of AQE and IQE. All samples contain 25 mol % Pt.

growth pattern (Volmer−Wever mode),[18] which differs from the layered overgrowth pattern (Frank−van der Merwe mode) of Ag on Au NRs. Pyramid-like Pt NPs with an edge length of ∼7 nm were homogeneously deposited on the Au NRs. In the extinction spectra (Figure 1b), an obvious decrease in LSPR intensity was observed because of the complete encapsulation of Au NR core by the Pt shell.[19] The Pt-tipped Au NRs were produced because of the close packing of the surface-capping surfactants at the sides of the Au NRs (Figure 1d). The Pt NPs selectively deposited at the ends also exhibited the pyramid-like structure. High-resolution transmission electron microscopy (HRTEM) images (Figures S4d and S6d) of both the Pt NPs and Au NRs showed coherent lattice fringes, suggesting an epitaxial growth of Pt on Au.[20] Such an epitaxial growth prevents defects and aids the formation of well-crystallized interfaces. The extinction spectrum of the Pt-tipped sample (Figure 1b) shows a strong red-shift and a broadening of the LSPR peak. The red-shift was attributed to the relative changes in the aspect ratio after tip coating.[21,22] FDTD simulation of the Pt-tipped Au NRs yielded consistent results (Figure S2b). Therefore, the enhanced absorption of the tip-coated sample will be beneficial for harvesting a wide range of visible−NIR light.

All the samples were treated with perchloric acid ($HClO_4$) to remove the surfactants that hinder the direct charge transfer between the catalyst and the adsorbed CH_3OH molecule (electron donor).[8] As shown in Figures S7a and S8a, the rate of H_2 evolution increased by two times after $HClO_4$ oxidation compared to Milli-Q water washing, suggesting that surfactant removal facilitated the charge-transfer process. Figure 2a shows the time-dependent profiles of H_2 production for different Pt-modified samples. Under visible-light irradiation, H_2 linearly evolved from the suspensions with increasing photoirradiation time. When compared with the Pt-covered Au NRs and Au nanospheres (NSs) (Figure S9), the Pt-tipped Au NRs exhibited a much higher rate of H_2 evolution. When the samples were observed in the dark (35 °C) for 6 h, no gas was evolved for any sample, indicating that no thermocatalytic H_2 was evolved under the present conditions.
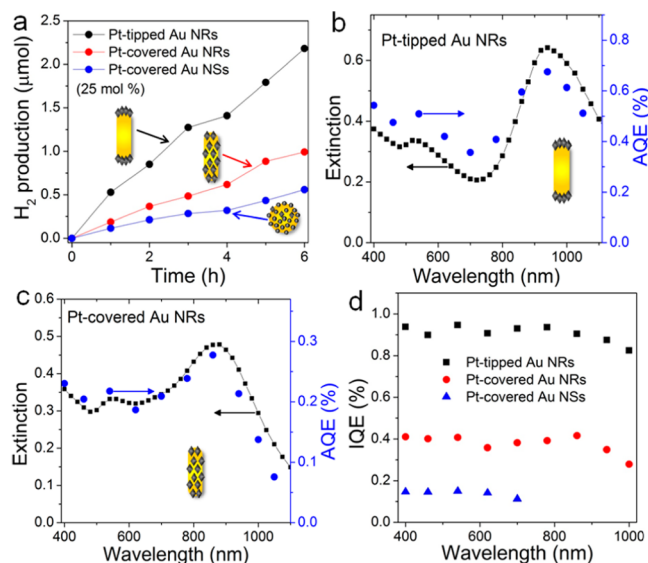
When monochromatic light with a width of ±5 nm and intensity of 2.6 mW cm^{-2} was irradiated at 298 K, H_2 was evolved, and the action spectrum was subsequently obtained. The apparent quantum efficiency (AQE) at each centered wavelength of the monochromatic light was calculated from the ratio of twice the number of H_2 molecules to the number of incident photons using the following equation: AQE = (2 × the number of H_2 molecules/the number of incident photons) × 100%. As shown in Figure 2b,c, the action spectra of AQE are in agreement with the absorption spectra of Pt-modified Au NRs. The AQE of Pt-tipped Au NRs reached 0.51% at 540 nm and 0.68% at 940 nm under the above conditions. Therefore, it can be concluded that H_2 evolution was induced by the SPR excitation of the Au NRs. Hydrogen overvoltage of Pt (0.01 V) was lower than that of Au (0.18 V), making electron transfer from Au to Pt possible.[23] Internal quantum efficiencies (IQE) of Pt-modified Au were compared to exclude the effect of light absorbance, as shown in Figure 2d. Interestingly, Pt-tipped Au NRs exhibited a much higher H_2-evolution rate compared to Pt-covered Au NRs and NSs. Therefore, Pt-tipped Au NRs show high catalytic activity because of their anisotropic heterostructure, which may facilitate the charge separation.

There are reports on the production of photocatalytic H_2 on Au/semiconductor composites utilizing the SPR of Au nanostructures.[12,24,25] However, the detailed mechanism of plasmon-induced electron transfer is still not clear, especially for the Au/metal system. Single-particle spectroscopy combined with morphological characterization is essential to investigate the interfacial electron transfer between Au NRs and Pt cocatalyst. To obtain the corresponding high-magnification morphology images, samples were spin coated on Al_2O_3/SiO_2-supported TEM grids, which were prepared by atomic layer deposition (Figure S10). Figure 3a shows a typical single-particle PL image of individual Au NRs; the high-magnification TEM images of the corresponding Au NRs are also displayed (see Figure S11 for the low-magnification TEM image). The excitation source was a circularly polarized 405 nm laser. The PL spectra of individual Au NRs are shown in Figure
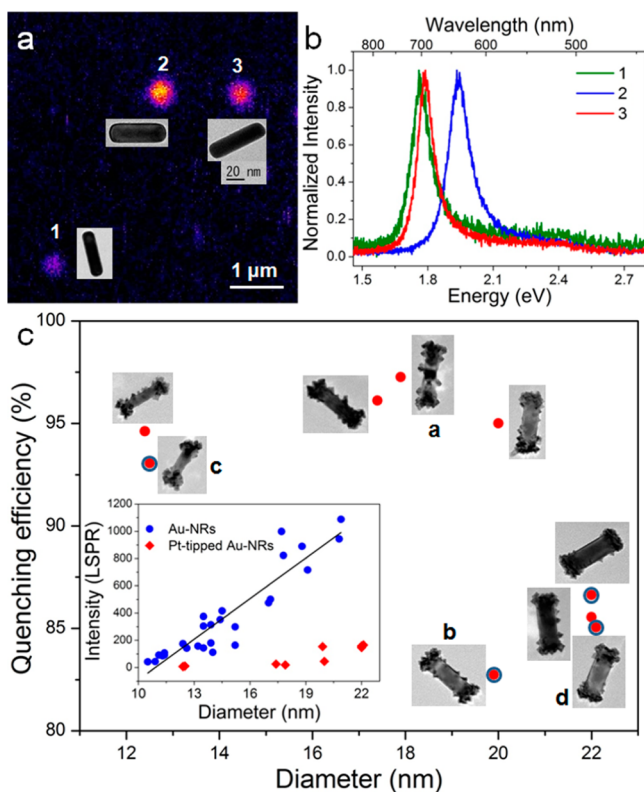
6871

dx.doi.org/10.1021/ja502704n | J. Am. Chem. Soc. 2014, 136, 6870−6873

Figure 3. (a) PL image of single Au NRs on a Al_2O_3–SiO_2-supported TEM grid. Correlated high-magnification TEM images are shown next to the PL signal. (b) Normalized PL spectra of the corresponding single Au NRs as numbered in the PL image. (c) PL quenching efficiency of individual Pt-tipped Au NRs. The circled points indicate the almost purely tip-coated samples. Inset: PL intensities as a function of diameter for individual Au NRs and Pt-tipped Au NRs.

3b. The peak position of the PL spectra at the LSPR region depends on the aspect ratio of the Au NRs. By analyzing the PL spectra for 27 Au NRs (Figure S12), we derived a good linear relationship between the LSPR maximum and the aspect ratio (Figure S13).

The PL images and spectra of the individual Pt-tipped Au NRs and their corresponding TEM images were obtained in the same manner (Figure S14 and S15). PL intensities at the LSPR and transversal surface plasmon resonance (TSPR) regions were obtained by fitting a Lorentzian line shape to the spectra of the Au NRs and Pt-tipped samples. As shown in the inset of Figure 3c, the LSPR PL intensity of the Pt-tipped samples dramatically decreased compared to Au NRs, while the TSPR PL intensity was similar for both the samples (Figure S16). This demonstrates that PL at the LSPR mode was quenched by the tip-coated Pt. The quenching efficiency of the individual Pt-tipped Au NRs was calculated by comparing the PL intensity of both the samples with the same diameter (Figure 3c). Because of the heterogeneity of the chemically synthesized NPs, a small number of Pt-tipped Au NRs were also laterally covered by Pt NPs, such as NR (a in Figure 3c), leading to a higher quenching efficiency (97%) than that (83%) of the almost purely tip-coated Au NRs (NR, b in Figure 3c), which only has few laterally covered Pt NPs. Furthermore, a comparison of the results of NR (c and d in Figure 3c) shows that the quenching efficiency is affected by diameter, as both the NRs have a purely tip-coated morphology. For Pt-covered Au NRs, the PL intensity was too low to be detected. Single-particle DFS

spectroscopy was further employed to investigate the electron transfer between Au NRs and Pt. The DFS spectra of the Pt-tipped sample also show a quenching phenomenon at the LSPR region (Figures S17 and S18). FDTD calculations reveal that the Pt-tipped nanostructure did not produce such strong quenching effect at the LSPR region (Figure S19). Therefore, it can be concluded that the quenching phenomenon arises as a consequence of the electron transfer from the excited Au NRs to Pt.

The PL of Au NRs has been attributed to the radiative decay of surface plasmon that occurs from both the TSPR and LSPR, the latter being the dominant decay channel.[26,27] In our single-particle PL experiments, the interband transition of Au NRs was excited to produce electron–hole pairs. A fast inter-conversion occurs between the electron–hole pairs and the TSPR that subsequently decays radiatively (luminous green line in Scheme 1), leading to the short-wavelength peak in the PL

Scheme 1. Schematic Diagram for Radiative Decay of Surface Plasmon (left) and Reaction Mechanism for H_2 Production (right)
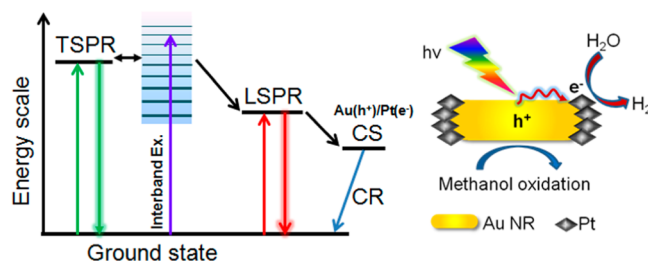
spectrum. Meanwhile, an energy transfer occurs from the TSPR to LSPR mode promoted by electron–hole pairs. Furthermore, the directly excited electrons might lose energy by nonradiative decay and interconvert to the LSPR mode,[28,29] which emits a photon via radiative decay (luminous red line). For the Pt-tipped Au NRs, the hot electrons that might get transferred from Au to Pt compete with the LSPR emission, leading to PL damping. The single-particle PL spectra showed quenching at the LSPR region, confirming the electron transfer from Au NRs to Pt. Under visible–NIR light irradiation, the hot electrons generated either by TSPR/LSPR excitation or interband excitation transfer to the tip-coated Pt, where H^+ reduces to H_2. The electron-transfer process involves a charge-separated state. Because the IQE of Pt-modified Au NRs for H_2 production was lower than 1%, charge recombination (CR) seems to be the dominant relaxation path (blue line in Scheme 1). The resulting electron-deficient Au NRs oxidize CH_3OH and return to their original metallic state. The spatial separation of reduction and oxidation sites in Pt-tipped Au NRs results in an efficient charge separation (CR) and, hence, an improved H_2 production (Scheme 1, right figure). For the Pt-covered Au NRs, the electron–hole pairs can easily recombine because of the homogeneous coating of Pt NPs.

In summary, Pt-modified Au NRs have been successfully synthesized by altering the side-coating surfactants. Among them, Pt-tipped Au NRs exhibited efficient photocatalytic H_2 evolution under visible–NIR light because the hot electrons arose from the excitation of surface plasmons in Au NRs. By combining single-particle spectroscopy with high-magnification TEM, we analyzed the quenching efficiency of individual Pt-tipped Au NRs with detailed morphological information, which

allowed us to understand the energy relaxation path of plasmon-generated hot electrons. The strong quenching of PL and light scattering at the LSPR region confirmed the electron transfer from Au NRs to Pt. FDTD calculations further supported our spectroscopic analyses. The findings obtained here may have great implications for plasmon-assisted photochemistry and provide insights into designing novel plasmonic photocatalysts.

■ ASSOCIATED CONTENT

Ⓢ Supporting Information

Experimental details, additional results of structural characterizations, single-particle PL and scattering spectra of the samples, and FDTD calculations. This material is available free of charge via the Internet at http://pubs.acs.org.

■ AUTHOR INFORMATION

Corresponding Author

tachikawa@port.kobe-u.ac.jp; majima@sanken.osaka-u.ac.jp

Present Address

†Department of Chemistry, Graduate School of Science, Kobe University, 1−1 Rokkodai-cho, Nada-ku, Kobe 657−8501, Japan

Notes

The authors declare no competing financial interest.

■ ACKNOWLEDGMENTS

■ REFERENCES

(1) Fujishima, A.; Honda, K. *Nature* **1972**, *238*, 37.
(2) Chen, X.; Mao, S. *Chem. Rev.* **2007**, *107*, 2891.
(3) Maeda, K.; Domen, K. *J. Phys. Chem. Lett.* **2010**, *1*, 2655.
(4) El-Sayed, M. A. *Acc. Chem. Res.* **2001**, *34*, 257.
(5) Burda, C.; Chen, X.; Narayanan, R.; El-Sayed, M. A. *Chem. Rev.* **2005**, *105*, 1025.
(6) Kelly, K. L.; Coronado, E.; Zhao, L. L.; Schatz, G. C. *J. Phys. Chem. B* **2003**, *107*, 668.
(7) Brus, L. *Acc. Chem. Res.* **2008**, *41*, 1742.
(8) Liu, L. Q.; Ouyang, S. X.; Ye, J. H. *Angew. Chem., Int. Ed.* **2013**, *52*, 6689.
(9) Pu, Y.-C.; Wang, G. M.; Chang, K.-D.; Ling, Y. C.; Lin, Y.-K.; Fitzmorris, B. C.; Liu, C.-M.; Lu, X. H.; Tong, Y. X.; Zhang, J. Z.; Hsu, Y.-J.; Li, Y. *Nano Lett.* **2013**, *13*, 3817.
(10) Linic, S.; Christopher, P.; Ingram, D. B. *Nat. Mater.* **2011**, *10*, 911.
(11) Hoggard, A.; Wang, L.-Y.; Ma, L. L.; Fang, Y.; You, G.; Olson, J.; Liu, Z.; Chang, W.-S.; Ajayan, P. M.; Link, S. *ACS Nano* **2013**, *7*, 11209.
(12) Tanaka, A.; Sakaguchi, S.; Hashimoto, K.; Kominami, H. *ACS Catal.* **2013**, *3*, 79.
(13) Chen, M. S.; Kumar, D.; Yi, C.-W.; Goodman, D. W. *Science* **2005**, *310*, 291.
(14) Wang, F.; Li, C.; Chen, H.; Jiang, R.; Sun, L.-D.; Li, Q.; Wang, J.; Yu, J. C.; Yan, C.-H. *J. Am. Chem. Soc.* **2013**, *135*, 5588.
(15) Guo, X.; Zhang, Q.; Sun, Y. H.; Zhao, Q.; Yang, J. *ACS Nano* **2012**, *2*, 1165.
(16) Wang, F.; Cheng, S.; Bao, Z. H.; Wang, J. F. *Angew. Chem., Int. Ed.* **2013**, *52*, 10344.
(17) Nikoobakht, B.; El-Sayed, M. A. *Langmuir* **2001**, *17*, 6368.
(18) Fan, F. R.; Liu, D. Y.; Wu, Y. F.; Duan, D.; Xie, Z. X.; Jiang, Z. Y.; Tian, Z. Q. *J. Am. Chem. Soc.* **2008**, *130*, 6949.
(19) Khanal, B. P.; Zubarev, E. R. *Angew. Chem., Int. Ed.* **2009**, *48*, 6888.
(20) Grzelczak, M.; Pérez-Juste, J.; Rodríguez-González, B.; Liz-Marzán, L. M. *J. Mater. Chem.* **2006**, *16*, 3946.
(21) Grzelczak, M.; Pérez-Juste, J.; García de Abajo, F. J.; Liz-Marzán, L. M. *J. Phys. Chem. C* **2007**, *111*, 6183.
(22) Fennell, J.; He, D. S.; Tanyi, A. M.; Logsdail, A. J.; Johnston, R. L.; Li, Z. Y.; Horswell, S. L. *J. Am. Chem. Soc.* **2013**, *135*, 6554.
(23) Tanaka, A.; Hashimoto, K.; Kominami, H. *J. Am. Chem. Soc.* **2014**, *136*, 586.
(24) Yuzawa, H.; Yoshida, T.; Yoshida, H. *Appl. Catal., B* **2012**, *115*, 294.
(25) Silva, C. G.; Juárez, R.; Marino, T.; Molinari, R.; García, H. *J. Am. Chem. Soc.* **2011**, *133*, 595.
(26) Bouhelier, A.; Bachelot, R.; Lerondel, G.; Kostcheev, S.; Royer, P.; Wiederrecht, G. P. *Phys. Rev. Lett.* **2005**, *95*, 267405.
(27) Tcherniak, A.; Dominguez-Medina, S.; Chang, W.-S.; Swanglap, P.; Slaughter, L. S.; Landes, C. F.; Link, S. *J. Phys. Chem. C* **2011**, *115*, 15938.
(28) Fang, Y.; Chang, W.-S.; Willingham, B.; Swanglap, P.; Dominguez-Medina, S.; Link, S. *ACS Nano* **2012**, *6*, 7177.
(29) Wackenhut, F.; Failla, A. V.; Meixner, A. J. *J. Phys. Chem. C* **2013**, *117*, 17870.